Light propagation in semi-infinite photonic crystals and related waveguide structures

Zhi-Yuan Li* and Kai-Ming Ho
Ames Laboratory and Department of Physics and Astronomy, Iowa State University, Ames, Iowa 50011, USA
(Received 11 April 2003; published 2 October 2003)

A transfer-matrix method (TMM) that employs the plane-wave expansion of electromagnetic (EM) fields has been developed to handle EM wave propagation in semi-infinite photonic crystal and related waveguide structures. The major aim is to account for wave scattering only at the concerned boundary and to completely remove multiple reflections in the presence of other structural boundaries. It turns out that the scattering problem is closely connected to the eigenmodes of the transfer matrix for the unit cell of the crystal. A natural boundary condition is imposed to describe the asymptotic propagation behavior of scattered EM waves in a region far away from the interface. Theories for a variety of important structures have been systematically set up. These include wave propagation in a semi-infinite photonic crystal, a coated semi-infinite photonic crystal, a heterostructure formed by two different semi-infinite photonic crystals face to face, and a complex sandwiched structure formed by two semi-infinite photonic crystals separated by a general grating slab. In combination with a supercell technique, the developed formulations can also be used to handle photonic crystal waveguide structures. We have applied the developed TMM to two-dimensional photonic crystal and related waveguide structures. The first is the coupling of an external wave into a photonic crystal (photonic crystal waveguide) and the related inverse problems of coupling of a Bloch's wave (guided wave) out of the photonic crystal (photonic crystal waveguide). The second is scattering of a guided wave by a cavity introduced into a photonic crystal waveguide. The developed TMM can help to understand optical properties and design optimal structures of individual functional elements in an optical integrated circuit built in a photonic crystal environment.

DOI: 10.1103/PhysRevB.68.155101 PACS number(s): 42.70.Qs, 41.20.Jb, 78.67.−n

I. INTRODUCTION

Photonic crystals are materials composed of periodic arrays of dielectric or metallic building blocks. They have attracted extensive interest in recent years because the existence of a photonic band gap (PBG) provides a novel way to control and mold the flow of electromagnetic (EM) waves much as conventional semiconductors to do electrons.[1,2] For instance, photonic crystals can serve as the platform for future electro-optic or all-optical ultrasmall integrated circuits (IC's), thanks to the peculiar propagation behavior of EM wave in defects introduced into photonic crystal structures. An optical IC can be made up of many different functional elements, among which are photonic crystal waveguides, waveguide bends and branches, and cavities.[3–14]

Understanding the propagation behavior of EM waves in these individual functional elements in the environment of an inhomogeneous medium, here a periodic photonic crystal, is of vital importance to assess the overall functionality and efficiency of an optical IC. It can also lay down the basis for further actively designing high-efficient circuits with more complicated configurations. The finite-different time-domain (FDTD) method[15] is a popular theoretical tool for this purpose. However, structural boundaries (such as exits of a photonic crystal waveguide) present in the FDTD simulations can lead to multiple-reflection phenomena that will entangle with useful information and then seriously contaminate the interpretation of the solution to the EM problems. For instance, when the FDTD technique is employed to treat coupling of EM wave into and out of a photonic crystal waveguide, the multiple reflection induced by second waveguide exit will greatly complicate the simulation. Another prominent example is the simulation of EM wave propagation through a waveguide sharp bend and calculation of the bending efficiency by means of the FDTD technique. In order to separate sufficiently the useful pulse and parasite multiple reflection pulses from two waveguide exits, very large simulation domain size must be adopted.[3] Artificial interfaces can be designed to connect these structural boundaries to the FDTD domain boundaries (usually the free space) to reduce the reflection.[16] However, they can hardly completely remove the multiple reflection and the design is not always easy for general structures. A naive while efficient and fundamental way to completely remove these multiple reflections is to adopt a structure without boundary. In our current problem this amounts to considering the problem of EM wave propagation through a semi-infinite photonic crystal structure in which no structural boundary exists and therefore no multiple reflection happens. In fact, this idea is not a new one. Recall the old classic problem in general optics of transmission and reflection of light through a glass plate. A useful insight into this problem is to first look at the transmission and reflection through an air-glass interface and contemporarily neglect the existence of the other air-glass interface. Then the glass plate can be assumed to be a semi-infinite medium. Further information from the multiple reflection between the two interfaces can be incorporated based on the knowledge for each single interface. Obviously, by adopting a semi-infinite glass medium, one has removed the entanglement with the multiple reflection effect, which can be troublesome when the glass plate is very thick. The same concept and principle also apply to our photonic crystal structures. It is helpful to only consider the single structural boundary in the first step and then add up multiple reflection

effect in the second step, if necessary.

Unlike a glass plate, the photonic crystal is a much more complicated inhomogeneous medium. At first glance, the problem seems to be much more difficult. However, after we go deep into analysis of this wave propagation problem we find that the fundamental concept used in the classic glass plate can also be utilized in the current complex structure. As we know, the usual way to solve wave propagation through a glass plate is to write down the eigenmodes in the glass plate (usually a transmission plane wave) and in air (incident and reflection plane waves), then to find out the coefficients of the eigenmodes by matching the boundary condition of EM fields at the interface. Energy conservation and lateral momentum conservation should be satisfied to yield the final answer. It turns out that the current problem of wave propagation through a semi-infinite photonic crystal can also be closely related to the eigenmodes in the photonic crystal. Unlike the simple eigenmode (plane wave function) in a homogeneous glass plate, the eigenmode in the photonic crystal is much more complex. Taking into account the principle of energy and lateral momentum conservation, the problem can be recast as: How to find the eigenmodes excited in the photonic crystal under an external incident wave at frequency ω and wave vector $\mathbf{k}_0$. We find that this problem can be conveniently solved in the general framework of the transfer-matrix formalism.[17–26] In this paper we will utilize the transfer-matrix method (TMM) on the basis of plane-wave expansion of EM fields since it provides an accurate way to deal with arbitrary photonic crystal structures.[21–26]

This paper is arranged as follows. In the next four sections, we will develop the TMM formalisms for wave scattering by different semi-infinite photonic crystal structures. In Sec. II we first consider the wave propagation in a semi-infinite photonic crystal structure surrounded by air or other homogeneous medium. This will lay down the theoretical foundation for later discussions on more complex structures. We also discuss how to solve efficiently the eigenmodes for the photonic crystal. In Sec. III we proceed to consider wave propagation through a semi-infinite photonic crystal coated with another general grating slab. In Sec. IV we consider wave propagation in a composite heterostructure consisting of two different semi-infinite photonic crystals face to face. Then in Sec. V we turn to a more complicated structure consisting of two different semi-infinite photonic crystals separated by a general grating slab, which we call a sandwiched structure. After we have settled the theoretical basis, we will take several examples of two-dimensional (2D) photonic cryptal and related waveguide structures to show the power of the developed theoretical tools. However, the developed method can equally apply to more complex 3D photonic crystal and related waveguide structures. In Sec. VI we consider a 2D photonic crystal composed of a square lattice of dielectric cylinders in air and see how an incident plane wave from the air side is scattered by this semi-infinite photonic crystal. The inverse process of a Bloch's wave incident from the semi-infinite photonic crystal side scattered by the air-crystal interface is also considered. In Sec. VII we apply the same theoretical tool to solve the problem of EM wave coupling into and out of a straight waveguide structure created in the above 2D photonic crystal. To appreciate the formulation of the TMM, a supercell technique is used. In Sec. VIII we focus on sandwiched structures consisting of two semi-infinite photonic crystal waveguides separated by localized defect structures. We consider an example of the scattering of an incident guided wave by a cavity placed between two identical semi-infinite waveguides. In Sec. IX we will further discuss the developed TMM in comparison with the popular FDTD techniques in application to design of functional elements in a photonic crystal based optical IC. Finally we will summarize this paper in Sec. X.

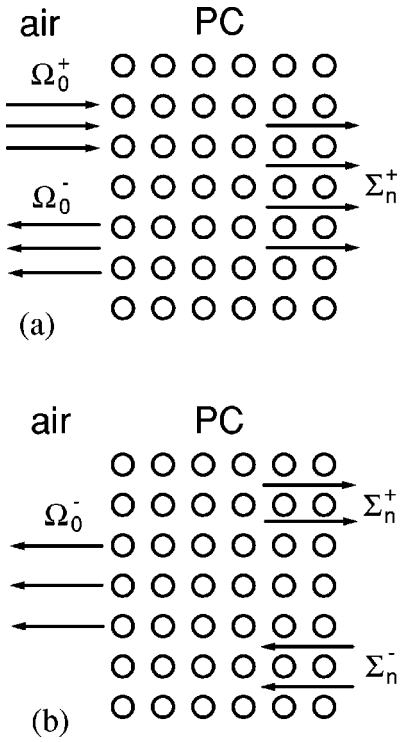

FIG. 1. Schematic configurations for (a) an external EM wave propagating from left to right scattered by a semi-infinite photonic crystal (PC) surrounded by air and (b) a Bloch wave propagating from right to left in the semi-infinite photonic crystal scattered by the air-crystal interface.

II. THEORY FOR WAVE PROPAGATION IN BARE SEMI-INFINITE PHOTONIC CRYSTAL STRUCTURES

To see how the problem of wave propagation in a semi-infinite photonic crystal structure is connected with the transfer matrix for the unit cell of the photonic crystal, let us first consider a simple case, where a plane EM wave with frequency ω_0 and wave vector $\mathbf{k}_0$ is incident in air from left to right along the z axis onto a semi-infinite photonic crystal. The configuration of this problem is schematically depicted in Fig. 1(a). The question is how to calculate the transmission field into the photonic crystal and the reflection field back into the air. Since this is essentially a scattering problem, we naturally turn to the TMM for answer. In addition, we adopt a plane wave basis to expand the EM fields, and assume that the left and right hand sides of each unit cell of

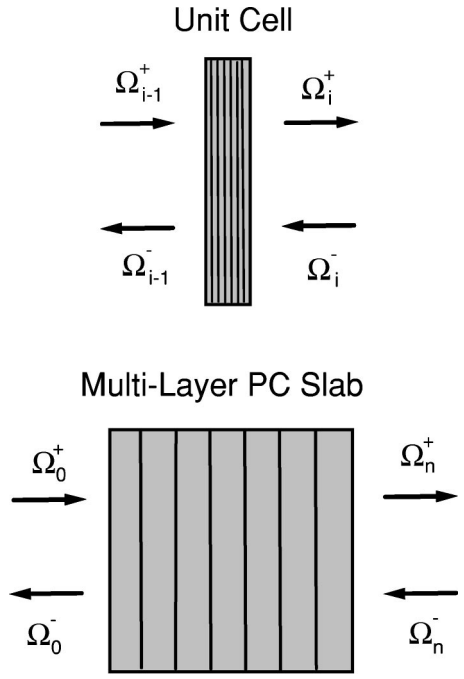

FIG. 2. Schematic configurations of EM wave propagation through (a) a single unit cell of a photonic crystal and (b) a photonic crystal slab consisting of n unit cells described by a transfer-matrix formalism in terms of column vectors $\Omega^{\pm}$, which are made up of plane wave coefficients of the EM fields.

the photonic crystal are surrounded by infinitely thin air films.[20,26] This means that all plane waves are placed in an air background, a natural selection to match the current problem that the semi-infinite photonic crystal is surrounded by an air background. This plane-wave basis will be adopted throughout all problems in this work.

It turns out that the EM fields at the right hand side of a single unit cell of the crystal can be connected with the fields at the left hand side (see the schematic configuration in the upper panel of Fig. 2) via a transfer matrix

$$\begin{pmatrix} \Omega_i^+ \\ \Omega_i^- \end{pmatrix} = T \begin{pmatrix} \Omega_{i-1}^+ \\ \Omega_{i-1}^- \end{pmatrix} = \begin{pmatrix} t_{11} & t_{12} \\ t_{21} & t_{22} \end{pmatrix} \begin{pmatrix} \Omega_{i-1}^+ \\ \Omega_{i-1}^- \end{pmatrix}. \tag{2.1}$$

Here Ω_i^+ (Ω_i^-) is a column vector composed of the expansion coefficients of the positive (negative) propagating plane wave in free space at the right hand side of the ith unit cell, while Ω_{i-1}^+ (Ω_{i-1}^-) is a column vector at the left hand side of the ith unit cell. For more detail of this transfer-matrix technique, the readers are referred to Ref. 26. T is called the transfer matrix (more accurately, the T matrix) for the ith crystal layer. With this transfer matrix T at hand and considering the periodicity of the photonic crystal, it can be shown that the fields after passing through n crystal layers (as depicted in the lower panel of Fig. 2) are given by

$$\begin{pmatrix} \Omega_n^+ \\ \Omega_n^- \end{pmatrix} = T^n \begin{pmatrix} \Omega_0^+ \\ \Omega_0^- \end{pmatrix}. \tag{2.2}$$

In this way, the EM fields inside the photonic crystal have been related to the fields at the air-crystal interface (with Ω_0^+ and Ω_0^- corresponding to the incident and reflection fields in air, respectively) through a new transfer matrix T^n.

Now we see that the matrix T plays a key role in determining how the wave propagates through the photonic crystal. Let us first have a closer look at it. From literatures one can find that in addition to its routine application in calculating transmission and reflection spectra, the TMM can also be used to solve the ordinary photonic band structures for a photonic crystal.[17–19,25,26] In doing so, one needs to impose the Bloch's boundary condition on the fields at the two hand sides of the unit cell

$$\begin{pmatrix} \Omega_i^+ \\ \Omega_i^- \end{pmatrix} = e^{i\mathbf{k}\cdot\mathbf{R}} \begin{pmatrix} \Omega_{i-1}^+ \\ \Omega_{i-1}^- \end{pmatrix}, \tag{2.3}$$

where $\mathbf{k}$ is the Bloch wave vector and $\mathbf{R}$ is the primitive lattice vector of the photonic crystal. This means that

$$T \begin{pmatrix} \Omega_{i-1}^+ \\ \Omega_{i-1}^- \end{pmatrix} = e^{i\mathbf{k}\cdot\mathbf{R}} \begin{pmatrix} \Omega_{i-1}^+ \\ \Omega_{i-1}^- \end{pmatrix}. \tag{2.4}$$

Therefore the Bloch phase factor is the eigenvalue of the matrix T. This suggests that we solve all the eigenvalues and eigenvectors of T, from which we have

$$TS = S\Lambda,$$

where Λ is a diagonal matrix composed of all eigenvalues $\{\lambda_i, i=1,\ldots,N\}$, with N being the dimension of T. S is a $N\times N$ matrix with its ith column being the eigenvector of T corresponding to the eigenvalue λ_i. Note that the Block's modes are among these eigenmodes for T. Now T can be expressed into $T=S\Lambda S^{-1}$, and Eq. (2.2) becomes

$$\begin{pmatrix} \Omega_n^+ \\ \Omega_n^- \end{pmatrix} = S\Lambda^n S^{-1} \begin{pmatrix} \Omega_0^+ \\ \Omega_0^- \end{pmatrix}. \tag{2.5}$$

From the eigenequation

$$T \begin{pmatrix} \Omega^+ \\ \Omega^- \end{pmatrix} = \lambda \begin{pmatrix} \Omega^+ \\ \Omega^- \end{pmatrix}, \tag{2.6}$$

we find

$$\Lambda\Sigma = \lambda\Sigma, \tag{2.7}$$

where $\Sigma = S^{-1}(\Omega^+, \Omega^-)^T$, with "$T$" denoting the matrix transposition. Ω^+ and Ω^- can be column vectors for any crystal layer.

Since Λ is a diagonal matrix, the eigenvector corresponding to λ_i should be $\Sigma = (0,\ldots,1,\ldots,0)^T$, namely, only one nonzero element is present at the ith row of the column vector. In fact, every element σ_i in a general column vector $\Sigma = \{\sigma_i, i=1,\ldots,N\}$ denotes an eigenmode of the transfer matrix T, whose eigenvalue is λ_i and whose amplitude is σ_i. This means that the column vector Σ has a very simple while elegant physical implication for the photonic crystal. We can see now that the unitary transformation S has served as a bridge to reflect the eigenmode in the original plane-wave

basis to that in the new eigenstate basis. Due to the significant simplicity of the new eigenstate basis, it is helpful to work closely in this space. Physically, due to the time-reversal symmetry of the structure, the eigenvalues of the transfer matrix should appear in pairs. Namely, once we have an eigenvalue λ_i, we should find another one $\lambda_j = 1/\lambda_i$.[19] This implies that each growing eigenvalue (and eigenmode) should one-to-one correspond to a decaying eigenvalue. In addition, each positive (forward) propagating Bloch's mode should also find a corresponding negative (backward) propagating Bloch's mode. Therefore, we can separate the eigenvalues λ into two classes, one class λ_+ corresponds to positive propagation modes, including those $|\lambda_+|<1$ (exponentially decaying) and positive propagating Bloch's modes, while the other class λ_- corresponds to negative propagation modes, including those $|\lambda_-|>1$ (exponentially growing) and negative propagating Bloch's modes. Correspondingly, the diagonal matrix Λ can be also separated into two parts, and thus can be rearranged into the following form:

$$\Lambda = \begin{pmatrix} \Lambda_+ & 0 \\ 0 & \Lambda_- \end{pmatrix}, \tag{2.8}$$

where Λ_+ and Λ_- correspond to the positive and negative eigenmodes, respectively. They should have same dimension. At the same time, the eigenvector matrix S should be rearranged in exactly the same way, namely, by exchanging different column vectors (eigenvectors) corresponding to λ_+ and λ_-. In our numerical practice, we find it very easy to separate exponentially growing or decaying modes by simply looking at the eigenvalue. However, special care must be taken to those Bloch's modes with $|\lambda| = 1$.[19] One can not simply judge the propagation direction of a Bloch's mode by looking at the Bloch's wave vector $\mathbf{k}_0$. Instead, the total energy flux along the z-axis direction should be calculated in a given plane, with the positive (negative) values corresponding to the positive (negative) propagating modes. Numerically this can be done from the plane wave coefficients involved in any column vectors Ω^+ and Ω^-, where only those propagating components corresponding to real k_z should be counted because of nonvanishing energy flux along the z axis. Due to the conservation of total energy flux along the z axis, any plane can be adopted.

With the new eigenstate basis at hand, we return back to our original scattering problem. Equation (2.5) can now be rewritten as

$$\Sigma_n = \Lambda^n \Sigma_0$$

or more explicitly

$$\begin{pmatrix} \Sigma_n^+ \\ \Sigma_n^- \end{pmatrix} = \begin{pmatrix} \Lambda_+^n & 0 \\ 0 & \Lambda_-^n \end{pmatrix} \begin{pmatrix} \Sigma_0^+ \\ \Sigma_0^- \end{pmatrix}, \tag{2.9}$$

which yields

$$\Sigma_n^+ = \Lambda_+^n \Sigma_0^+, \quad \Sigma_n^- = \Lambda_-^n \Sigma_0^-. \tag{2.10}$$

This amounts to first projecting the incident field from original plane-wave basis onto the eigenmode space, then each eigenmode propagates through the photonic crystal without changing its state. For a semi-infinite photonic crystal structure, there is no boundary to reflect the forward propagating eigenmodes into the backward propagating modes. This physical intuition imposes a natural boundary condition for our scattering problem: All backwards propagating modes within the photonic crystal are exactly zero. Therefore, $\Sigma_n^- = 0$, which also means that $\Sigma_0^- = (\Lambda_-)^{-n} \Sigma_n^- = 0$. In addition, according to the first equation in Eq. (2.10), all positive propagating mode will decay to null except those Bloch modes with $|\lambda_+| = 1$ after they travel past a long distance along the z-axis direction. For the time being, let us suppose only one single Bloch mode is excited inside the photonic crystal at ω_0 and $\mathbf{k}_0$ (whose component parallel to the surface of the photonic crystal should be conserved during the scattering process). Let the Bloch phase factor be denoted by $\exp(i\mathbf{k}_0 \cdot \mathbf{R}) = \lambda_j$. From equality

$$S^{-1} \begin{pmatrix} \Omega_0^+ \\ \Omega_0^- \end{pmatrix} = \begin{pmatrix} \Sigma_0^+ \\ \Sigma_0^- \end{pmatrix} \tag{2.11}$$

we derive

$$\Omega_0^+ = S_{11} \Sigma_0^+, \quad \Omega_0^- = S_{21} \Sigma_0^+,$$

from which we get

$$\Sigma_0^+ = S_{11}^{-1} \Omega_0^+, \quad \Sigma_n^+ = \Lambda_+^n \Sigma_0^+ = \Lambda_+^n S_{11}^{-1} \Omega_0^+. \tag{2.12}$$

The reflection field in the plane wave basis is written as

$$\Omega_0^- = S_{21} \Sigma_0^+ = S_{21} S_{11}^{-1} \Omega_0^+, \tag{2.13}$$

and the transmission field is

$$\Omega_n^+ = S_{11} \Sigma_n^+, \quad \Omega_n^- = S_{21} \Sigma_n^+. \tag{2.14}$$

The transmission field is consisting of both the Bloch mode and all other evanescent modes. At a plane very far away from the air-crystal interface, only the Bloch mode survives, and we have $\Sigma_n^+ = [0, \ldots, 0, (\lambda_j)^n (S_{11}^{-1} \Omega_0^+)_j, 0, \ldots, 0]^T$. Equations (2.12)–(2.14) are the final answer to our scattering problem. Using the plane-wave expansion coefficients, one can calculate the total energy flux for the Bloch wave, and thus the transmission coefficient. This can be done either in $\mathbf{k}$ space or in real space. The same procedure can apply to the reflection field and the reflection coefficient for the energy flux.

In the above we consider a plane wave incident from the air side onto the semi-infinite photonic crystal. The idea and formulation developed can also be applied to solve the inverse problem, namely, how an EM wave propagating from deep inside the photonic crystal incident onto the air-crystal interface is scattered by the interface. The configuration of this problem is schematically depicted in Fig. 1(b). From the above analysis we know that the wave mode that can exist within deep inside the photonic crystal must be a Bloch mode. Suppose the Bloch mode is at a frequency ω_0 and a Bloch wave vector $\mathbf{k}_0$, then the corresponding eigenvalue of the transfer matrix T is $\lambda_j = \exp(i\mathbf{k}_0 \cdot \mathbf{R})$. Part of the wave will transmit through the interface into the air region, other

part will be reflected back into the semi-infinite photonic crystal, and finally evolve into another Bloch mode. According to Eq. (2.10), we have

$$\Sigma_0^- = (\Lambda_-)^{-n}\Sigma_n^- . \tag{2.15}$$

So if we write $\Sigma_n^- = (0,\ldots,0,\sigma_j^-,0,\ldots,0)^T$, then $\Sigma_0^- = [0,\ldots,0,\sigma_j^-(\lambda_j)^{-n},0,\ldots,0]^T$. From the transformation (2.11) and the fact that in the air region $\Omega_0^+ = 0$ (no reflection waves), we have

$$\Sigma_0^- = Q_{22}\Omega_0^- , \quad \Sigma_0^+ = Q_{12}\Omega_0^- , \tag{2.16}$$

where $Q = S^{-1}$. From Eq. (2.16) we find that the transmission field in the air region is given by

$$\Omega_0^- = Q_{22}^{-1}\Sigma_0^- . \tag{2.17}$$

From Eqs. (2.16) and (2.17) we find $\Sigma_0^+ = Q_{12}Q_{22}^{-1}\Sigma_0^-$, from which the field reflected into the photonic crystal is found to be $\Sigma_n^+ = \Lambda_+^n\Sigma_0^+$ in the eigenmode space, and the corresponding plane-wave expansion form is given by Eq. (2.14).

How if the background surrounding the semi-infinite photonic crystal is a general homogeneous material other than air? The problem can be solved by introducing a T matrix for the air and homogeneous medium interface T_m. Let the field in the homogeneous medium be $\Omega_m^{\pm}$, which is related to $\Omega_0^{\pm}$ by $(\Omega_m^+,\Omega_m^-)^T = T_m(\Omega_0^+,\Omega_0^-)^T$. The scattering problem now can be solved by simply replacing the eigenvector matrix S in Eqs. (2.11)–(2.17) by $T_m S$, for both situations of incidence.

In the above discussions, we have observed that the eigenvalues and eigenvectors of the T matrix for a unit cell play a key role in solution of the scattering problem. Numerically, to calculate this T matrix, we usually cut the unit cell into a number of thin slices along the z-axis direction, as shown in the upper panel of Fig. 2. Each of these slices is assumed to be a lamellar grating, for which Maxwell's equations can be solved and the transfer matrix connecting the fields at the two hand sides of this grating obtained. The total T matrix is a simple multiplication of all the single-slice transfer matrices. Another numerically more stable way is to use the scattering-matrix (S-matrix) formulation. The S matrix for each thin slice can be solved in a similar way to the T matrix,[26] and the S matrix for the unit cell can be calculated from these individual S matrices through a simple recursion algorithm.[17,22,26] The S matrix for the unit cell S_u is defined as

$$\begin{pmatrix} \Omega_i^+ \\ \Omega_{i-1}^- \end{pmatrix} = S_u \begin{pmatrix} \Omega_{i-1}^+ \\ \Omega_i^- \end{pmatrix} = \begin{pmatrix} S_u^{(11)} & S_u^{(12)} \\ S_u^{(21)} & S_u^{(22)} \end{pmatrix} \begin{pmatrix} \Omega_{i-1}^+ \\ \Omega_i^- \end{pmatrix}, \tag{2.18}$$

where $S_u^{(ij)}$ (i,j=1,2) are four block submatrices of S_u. The eigenproblem can be cast into the following form:

$$\begin{pmatrix} S_u^{(11)} & 0 \\ S_u^{(21)} & -I \end{pmatrix} \begin{pmatrix} \Omega_{i-1}^+ \\ \Omega_{i-1}^- \end{pmatrix} = \lambda \begin{pmatrix} I & -S_u^{(12)} \\ 0 & -S_u^{(22)} \end{pmatrix} \begin{pmatrix} \Omega_{i-1}^+ \\ \Omega_{i-1}^- \end{pmatrix}. \tag{2.19}$$

We recognize that Eq. (2.19) is a standard form of generalized eigenproblem $Ax = \lambda Bx$, where A and B are both square matrices, λ is the eigenvalue, and x is the eigenvector. So we can use some standard eigensolution algorithms to solve the eigenvalues and eigenvectors of Eq. (2.19).

Under given ω_0 and $\mathbf{k}_0$ for an incident wave, the number of Bloch modes that can be excited is limited to two or several. Most eigenmodes for the transfer matrix T or S are nonpropagation (evanescent) modes. The maximum $|\lambda_m|$ (corresponding to the strongest decaying modes) is almost proportional to the plane wave number used, $|\lambda_m| \approx e^{|\mathbf{G}_m|}$, where $|\mathbf{G}_m|$ is the maximum modulus of the reciprocal lattice vectors, and is approximately proportional to the plane-wave number. According to our numerical practice, when the number of plane wave is not too large, so that $|\lambda_m| < 10^{14}$, all eigenmodes calculated from the S-matrix formulation are identical to those obtained from the T-matrix formulation to a very high accuracy, especially for the Bloch modes and other nonpropagation modes with $|\lambda|$ closest to 1. In addition, λ_+ and λ_- have equal numbers, and $\lambda_+ = 1/\lambda_-$ is satisfied one-to-one to a high accuracy. However, when the plane-wave number is increased to a large value in order to guarantee a good convergence of numerical solution, numerical overflow or underflow begins to take effect in solution of eigenproblem by means of either Eq. (2.6) or (2.19), although the eigenvalues and eigenvectors for the Bloch's modes are not affected. λ_+ and λ_- no longer have equal numbers, and $\lambda_+ = 1/\lambda_-$ is not satisfied for very large $|\lambda|$. To overcome these difficulties, we consider another equivalent form of eigenproblem based on the S-matrix algorithm of Eq. (2.19). Instead of directly solving the eigenvalue λ, we turn to solving $(\lambda+1)^{-1}$, which does not cause overflow or underflow for $|\lambda| \gg 1$ or $|\lambda| \ll 1$. Similar technique has been employed in Ref. 25. In our numerical practice, it is very rare that λ is extremely close to -1, so that $(\lambda+1)^{-1}$ will never overflow. From the equality $Ax = \lambda Bx$, we can derive $Bx = (\lambda+1)^{-1}(A+B)x$, or equivalently from Eq. (2.19) we can find the following numerically more stable eigenproblem:

$$\begin{pmatrix} I & -S_u^{(12)} \\ 0 & -S_u^{(22)} \end{pmatrix} \begin{pmatrix} \Omega_{i-1}^+ \\ \Omega_{i-1}^- \end{pmatrix} = (\lambda+1)^{-1} \begin{pmatrix} I+S_u^{(11)} & -S_u^{(12)} \\ S_u^{(21)} & -I-S_u^{(22)} \end{pmatrix} \times \begin{pmatrix} \Omega_{i-1}^+ \\ \Omega_{i-1}^- \end{pmatrix}. \tag{2.20}$$

Obviously, the eigenvectors solved from Eq. (2.20) or Eq. (2.19) are same as those solved from Eq. (2.6), and can be used to construct the important eigenvector matrix S in Eqs. (2.5) and (2.11).

In the above discussions, we have extended the conventional TMM from its standard application to calculate the transmission and reflection spectra for a photonic crystal slab (more generally, a grating slab) to the current wave propagation in semi-infinite photonic crystal structures. Since the photonic crystal slab is usually thick compared to the wavelength, the numerically stable S-matrix formulation is dominantly used in favor of the T-matrix formulation. In practice, an efficient layer-doubling algorithm has been routinely uti-

lized to extract the overall *S* matrix for the whole slab from the *S* matrices for all the individual composite layers.[17–26] In the case of a photonic crystal slab, the *S* matrix for a unit cell plays a key role; the same as in the current semi-infinite structures. However, the TMM developed for a finite slab cannot be directly applied to a semi-infinite structure. The reason is simple. In a finite slab, no matter how thick it is, there always exist two air-crystal interfaces. Consequently multiple reflections are always present within the slab, and they become more violent for thicker slabs. Since the usage of the *S*-matrix algorithm has automatically involved these multiple reflections, the solution to a very thick slab (even approaching infinitely thick) does not converge to the true wave problem for a semi-infinite structure, where no multiple reflections are present. Physically, these multiple reflections will make it difficult to extract the transmission and reflection properties of the single air-crystal interface from the overall spectra for the whole slab calculated by the conventional TMM. It is easy to retrieve the overall spectrum information of the whole slab from those for the individual interface, but hard or even impossible to do the inverse, especially for more complex structures involving many interfaces. This fact has been well recognized when one tries to apply the FDTD technique to integrated optical elements.[3,16]

One might assume that introduction of a slight absorption into the photonic crystal structure, either from consideration of the absorptive properties of realistic optical materials or for the sake of numerical convenience, can remove the multiple reflections from the second air-crystal interface of a very thick crystal slab. By doing so, the reflection properties of a thick crystal slab will approach those of a semi-infinite crystal structure, and they can be readily solved by the conventional TMM for a finite crystal slab. However, this scheme can only apply to the simplest problem of an incident EM waves from the air side reflected by the air-crystal interface, as shown in Fig. 1(a). For the inverse problem for a Bloch's wave scattered by the air-crystal interface as shown in Fig. 1(b), the introduction of absorption into the photonic crystal will render the problem ill imposed, because no wave can reach the air-crystal interface due to absorption of EM waves after passing a long path through the thick crystal slab. When one considers more complicated semi-infinite photonic crystal structures such as a sandwiched structure (as shown in Fig. 5) that will be discussed in Sec. V, the limitation of this absorption scheme will become more evident. Therefore, the scheme of removing multiple reflections within a photonic crystal by introducing absorption proves not to be an optimum and effective scheme to handle complex photonic crystal functional elements.

III. THEORY OF WAVE PROPAGATION IN COATED SEMI-INFINITE PHOTONIC CRYSTAL STRUCTURES

In the last section, we consider EM wave scattering by a bare semi-infinite photonic crystal surrounded by air or another homogeneous medium background. In this section we consider a semi-infinite photonic crystal coated with a general periodic structure, which can be either a photonic crystal slab, a general grating, or simply a homogeneous medium

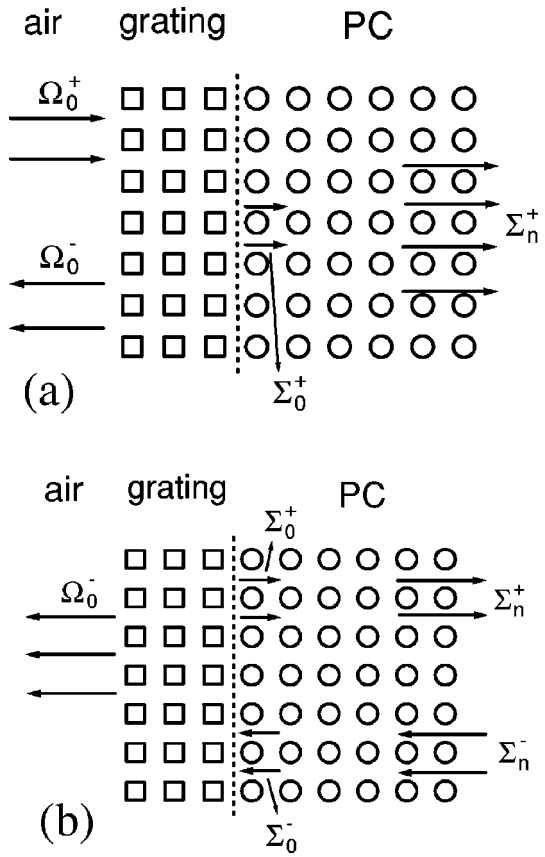

FIG. 3. Schematic configurations for (a) scattering of an external EM wave by a semi-infinite photonic crystal coated with a grating slab; (b) scattering of a Bloch wave in the coated semi-infinite photonic crystal.

slab. In the case of a periodic structure, the lattice in the lateral *XOY* plane must match with that of the semi-infinite photonic crystal in both the lattice type and lattice constant, so that the TMM formalism can be employed.

The schematic configuration of this scattering problem is depicted in Fig. 3. In Fig. 3(a), a plane wave is incident from left to right onto the coated layer. One part of the wave is reflected, the other transmits through the coated layer and finally evolves into the semi-infinite photonic crystal as a Bloch wave. The fields at the surface of the coated layer and the interface between the photonic crystal and the coated layer [represented by a dashed line in Fig. 3(a)] are denoted as $\Omega_0^{\pm}$ and $\Omega_1^{\pm}$. These fields are connected with each other through an *S* matrix S_a,

$$\begin{pmatrix} \Omega_1^+ \\ \Omega_0^- \end{pmatrix} = S_a \begin{pmatrix} \Omega_0^+ \\ \Omega_1^- \end{pmatrix} = \begin{pmatrix} S_a^{(11)} & S_a^{(12)} \\ S_a^{(21)} & S_a^{(22)} \end{pmatrix} \begin{pmatrix} \Omega_0^+ \\ \Omega_1^- \end{pmatrix}. \tag{3.1}$$

For the semi-infinite photonic crystal, we have the following relation:

$$\begin{pmatrix} \Omega_1^+ \\ \Omega_1^- \end{pmatrix} = S \begin{pmatrix} \Sigma_0^+ \\ \Sigma_0^- \end{pmatrix} = \begin{pmatrix} S_{11} & S_{12} \\ S_{21} & S_{22} \end{pmatrix} \begin{pmatrix} \Sigma_0^+ \\ \Sigma_0^- \end{pmatrix}, \tag{3.2}$$

where $\Sigma_0^{\pm}$ are coefficients of the eigenmode of the photonic crystal and *S* is the corresponding eigenvector matrix. We

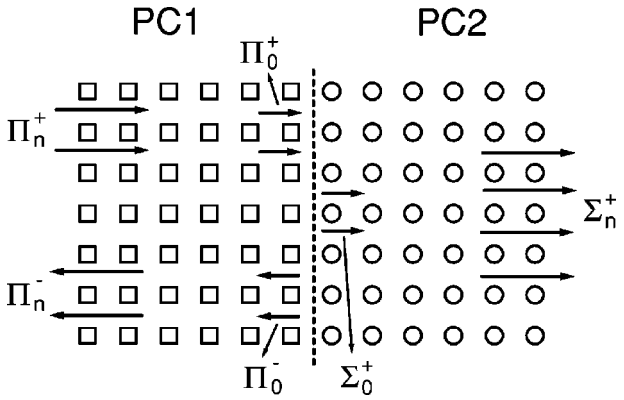

FIG. 4. Schematic configuration of EM wave propagating in a heterostructure consisting of two different semi-infinite photonic crystals face to face.

impose the natural boundary condition deep inside the photonic crystal $\Sigma_0^- = \Sigma_n^- = 0$. This leads to $\Omega_1^+ = S_{11}\Sigma_0^+$, and $\Omega_1^- = S_{21}\Sigma_0^+$. Substituting them into Eq. (3.1), we have

$$[S_{11} - S_a^{(12)} S_{21}]\Sigma_0^+ = S_a^{(11)}\Omega_0^+, \tag{3.3}$$

$$\Omega_0^- = S_a^{(21)}\Omega_0^+ + S_a^{(22)} S_{21}\Sigma_0^+. \tag{3.4}$$

The reflection field (Ω_0^-) and transmission field (Σ_0^+) can be solved directly from Eqs. (3.3) and (3.4). Similar to the procedure in Sec. II, the transmission field Σ_n^+ deep inside the photonic crystal Σ_n^+ can be connected to Σ_0^+ through free propagation of each eigenmode, and only the Bloch modes can survive after such a long path of propagation.

We can also consider the inverse process, namely, a Bloch wave, which is described by a column vector in the eigenstate space $\Sigma_n^- = (0, \ldots, 0, \sigma_j^-, 0, \ldots, 0)^T$, is incident from right to left onto the interface between the coated layer and the photonic crystal, as shown schematically in Fig. 3(b). One part of wave is reflected back into the crystal, the other transmits through the coated layer into the air background. In such a situation, we have $\Omega_0^+ = 0$. Then from Eq. (3.1) we find $\Omega_1^+ = S_a^{(12)}\Omega_1^-$, $\Omega_0^- = S_a^{(22)}\Omega_1^-$. Substituting them into Eq. (3.2), we have the following linear equations:

$$\begin{pmatrix} S_{11} & -S_a^{(12)} \\ S_{21} & -I \end{pmatrix} \begin{pmatrix} \Sigma_0^+ \\ \Omega_1^- \end{pmatrix} = \begin{pmatrix} S_{12}\Sigma_0^- \\ S_{22}\Sigma_0^- \end{pmatrix}. \tag{3.5}$$

After solution of Σ_0^+ and Ω_1^-, the reflection field into the photonic crystal (described by Σ_0^+ and Σ_n^+) and the transmission field into air, which is given by $\Omega_0^- = S_a^{(22)}\Omega_1^-$, are readily known.

IV. THEORY OF WAVE PROPAGATION IN PHOTONIC CRYSTAL HETEROSTRUCTURES

In the above sections we consider wave propagation in a composite infinite system composed of a semi-infinite air (or other homogeneous medium) background and a semi-infinite photonic crystal structure (either bare or coated). Now we push one step further to investigate a heterostructure formed by two different semi-infinite photonic crystal structures in touch face to face. The schematic configuration of the system is displayed in Fig. 4. The two semi-infinite photonic crystal should also have the same lattice structure (the same lattice type and lattice constants) in the lateral *XOY* plane, in order that the whole system can be assumed as a grating (infinitely thick) to allow for application of the conventional TMM formulation.

Suppose that we have already solved the eigenmodes of the *T* matrix (or *S* matrix) in the semi-infinite photonic crystals 1 and 2, following the procedures described in Sec. II. In the semi-infinite photonic crystal 1, we have

$$T_1 = S_1\Lambda_1 S_1^{-1}, \quad S_1^{-1}\begin{pmatrix} \Omega_1^+ \\ \Omega_1^- \end{pmatrix} = \begin{pmatrix} \Pi^+ \\ \Pi^- \end{pmatrix} \tag{4.1}$$

and

$$\Pi_0^+ = \Lambda_{1,+}^n \Pi_n^+, \quad \Pi_0^- = \Lambda_{1,-}^n \Pi_n^-. \tag{4.2}$$

In the semi-infinite photonic crystal 2, we have

$$T_2 = S_2\Lambda_2 S_2^{-1}, \quad S_2^{-1}\begin{pmatrix} \Omega_2^+ \\ \Omega_2^- \end{pmatrix} = \begin{pmatrix} \Sigma^+ \\ \Sigma^- \end{pmatrix} \tag{4.3}$$

and

$$\Sigma_n^+ = \Lambda_{2,+}^n \Sigma_0^+, \quad \Sigma_n^- = \Lambda_{2,-}^n \Sigma_0^-. \tag{4.4}$$

The same fields at the interface (denoted by the dashed line in Fig. 4) between the two semi-infinite photonic crystals can be written either in reference to the eigenstate space for the semi-infinite crystal on the left hand side or to the eigenstate space for the crystal on the right hand side. This leads to the following equality:

$$\begin{pmatrix} \Omega_{2,0}^+ \\ \Omega_{2,0}^- \end{pmatrix} = \begin{pmatrix} \Omega_{1,0}^+ \\ \Omega_{1,0}^- \end{pmatrix}. \tag{4.5}$$

To solve the scattering problem, we need to impose a natural boundary condition that $\Sigma_n^- = 0$ at $z = +\infty$. This immediately yields $\Sigma_0^- = 0$. From Eq. (4.5) we get

$$S_2\begin{pmatrix} \Sigma_0^+ \\ \Sigma_0^- \end{pmatrix} = S_1\begin{pmatrix} \Pi_0^+ \\ \Pi_0^- \end{pmatrix},$$

which yields

$$\begin{pmatrix} \Pi_0^+ \\ \Pi_0^- \end{pmatrix} = P\begin{pmatrix} \Sigma_0^+ \\ \Sigma_0^- \end{pmatrix}, \tag{4.6}$$

where $P = (S_1)^{-1}S_2$. From the fact that $\Sigma_0^- = 0$ we can write

$$\Pi_0^+ = P_{11}\Sigma_0^+, \quad \Pi_0^- = P_{21}\Sigma_0^+. \tag{4.7}$$

In combination of Eq. (4.2), we find

$$\Sigma_0^+ = (P_{11})^{-1}\Lambda_{1,+}^n \Pi_n^+. \tag{4.8}$$

The transmission and reflection fields can be directly calculated from Σ_0^+,

$$\Pi_n^- = (\Lambda_{1,-}^n)^{-1}\Pi_0^- = (\Lambda_{1,-}^n)^{-1}P_{21}\Sigma_0^+, \tag{4.9}$$

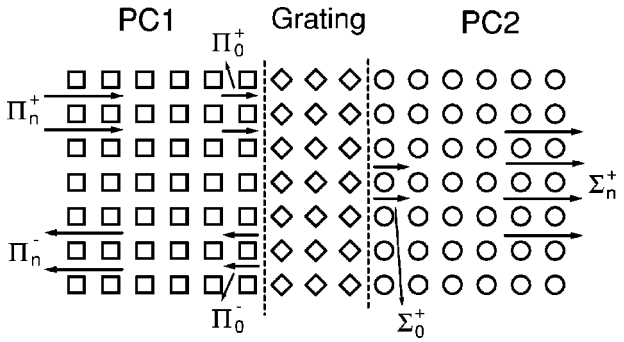

FIG. 5. Schematic configuration of EM wave propagating in a complex sandwiched structure consisting of two semi-infinite photonic crystals separated by a general grating slab.

$$\Sigma_n^+ = \Lambda_{2,+}^n \Sigma_0^+ . \tag{4.10}$$

The field distribution in the real space can then be evaluated from the plane-wave expansion of the eigenmodes using Eqs. (4.1) and (4.3). Therefore, given an incident Bloch mode $\Pi_n^+ = (0, \ldots, 0, \pi_j^+, 0, \ldots, 0)^T$, we can calculate the reflection and transmission fields in the two hand sides of the photonic crystal heterostructure. These fields should correspond to the Bloch wave propagation in each photonic crystal when far away from the interface.

V. THEORY OF WAVE PROPAGATION IN SANDWICHED PHOTONIC CRYSTAL STRUCTURES

Now suppose that the two semi-infinite photonic crystals do not directly touch face to face, but are separated by a sandwiched structure, as shown schematically in Fig. 5. The central sandwiched structure can be a simple homogeneous medium slab, a general grating slab, or another photonic crystal slab. We also require that the sandwiched slab should have the same lattice structure as the two semi-infinite photonic crystals in the lateral *XOY* plane.

The solution follows a very similar procedure to that for the heterostructure discussed in Sec. IV. Instead of Eq. (4.5), the fields at the surface of the left photonic crystal and the fields at the surface of the right photonic crystal (which are also the left and right surface of the sandwiched slab) are now connected by a transfer matrix T_a (a T matrix) as

$$\begin{pmatrix} \Omega_{2,0}^+ \\ \Omega_{2,0}^- \end{pmatrix} = T_a \begin{pmatrix} \Omega_{1,0}^+ \\ \Omega_{1,0}^- \end{pmatrix}. \tag{5.1}$$

Then we get

$$\begin{pmatrix} \Pi_0^+ \\ \Pi_0^- \end{pmatrix} = P \begin{pmatrix} \Sigma_0^+ \\ \Sigma_0^- \end{pmatrix}, \tag{5.2}$$

where $P = (S_1)^{-1}(T_a)^{-1}S_2$. The subsequent derivations are exactly identical to Eqs. (4.7)–(4.10) in Sec. IV. Therefore, given an incident Bloch mode at $z = -\infty$ of the left photonic crystal structure, which corresponds to a column vector in the eigenstate space for this photonic crystal as $\Pi_n^+ = (0, \ldots, 0, \pi_j^+, 0, \ldots, 0)^T$, we can calculate the reflection field and the transmission field scattered by the sandwiched structure. The scattered EM fields also correspond to the Bloch's wave propagation in each photonic crystal when far away from the sandwiched structure.

When the central sandwiched slab is thick, the algorithm to derive the T matrix T_a is numerically unstable. So, we need to take another stable algorithm, the S-matrix algorithm. Let the S matrix for the total slab be S_a, which satisfies

$$\begin{pmatrix} \Omega_{2,0}^+ \\ \Omega_{1,0}^- \end{pmatrix} = S_a \begin{pmatrix} \Omega_{1,0}^+ \\ \Omega_{2,0}^- \end{pmatrix}. \tag{5.3}$$

According to Eqs. (4.1) and (4.3), the column vectors in the both hand sides are related to the eigenmodes of the two photonic crystals by

$$\Omega_{2,0}^+ = S_2^{(11)}\Sigma_0^+ , \quad \Omega_{2,0}^- = S_2^{(21)}\Sigma_0^+ ,$$

$$\Omega_{1,0}^+ = S_1^{(11)}\Pi_0^+ + S_1^{(12)}\Pi_0^- , \quad \Omega_{1,0}^- = S_1^{(21)}\Pi_0^+ + S_1^{(22)}\Pi_0^- , \tag{5.4}$$

where $S_1^{(ij)}$ and $S_2^{(ij)}$ $(i,j=1,2)$ are the block submatrices of S_1 and S_2. In deriving Eq. (5.4), we have considered the fact that $\Sigma_0^- = 0$, and Π_0^+ has already been known from the coefficient of the incident Bloch mode Π_n^+ $(\Pi_0^+ = \Lambda_{1,+}^n \Pi_n^+)$. Combining Eqs. (5.3) and (5.4), we have

$$\begin{pmatrix} 0 \\ S_1^{(21)}\Pi_0^+ \end{pmatrix} + \begin{pmatrix} S_2^{(11)} & 0 \\ 0 & S_1^{(22)} \end{pmatrix} \begin{pmatrix} \Sigma_0^+ \\ \Pi_0^- \end{pmatrix} = S_a \begin{pmatrix} S_1^{(11)}\Pi_0^+ \\ 0 \end{pmatrix} + S_a \begin{pmatrix} 0 & S_1^{(12)} \\ S_2^{(21)} & 0 \end{pmatrix} \begin{pmatrix} \Sigma_0^+ \\ \Pi_0^- \end{pmatrix} \tag{5.5}$$

from which we obtain the following linear equations:

$$\begin{pmatrix} S_2^{(11)} - S_a^{(12)}S_2^{(21)} & -S_a^{(11)}S_1^{(12)} \\ -S_a^{(22)}S_2^{(21)} & S_1^{(22)} - S_a^{(21)}S_1^{(12)} \end{pmatrix} \begin{pmatrix} \Sigma_0^+ \\ \Pi_0^- \end{pmatrix} = \begin{pmatrix} S_a^{(11)}S_1^{(11)}\Pi_0^+ \\ [S_a^{(21)}S_1^{(11)} - S_1^{(21)}]\Pi_0^+ \end{pmatrix}. \tag{5.6}$$

In Eq. (5.6), $S_a^{(ij)}$ $(i,j=1,2)$ are the block submatrices of the S matrix S_a. The unknown variables Σ_0^+ and Π_0^- can be solved by standard technique such as Gaussian elimination method. After they are solved, the coefficients of the reflection and transmission Bloch modes in the two photonic crystals can be obtained by using Eqs. (4.9) and (4.10). Then the reflection and transmission fields as well as the total energy flux of these fields are readily calculated, from which we can obtain the knowledge of transmission and reflection coefficients.

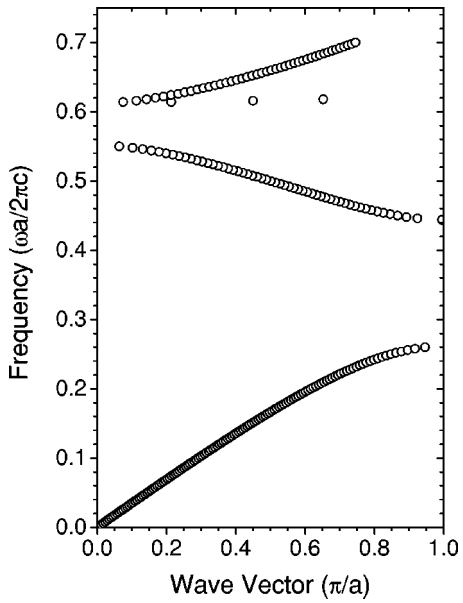

FIG. 6. Plots of the photonic band structures along the (10) direction of a 2D photonic crystal. The crystal is composed of a square lattice of dielectric cylinder in air with parameters $\epsilon = 11.56$ and $r = 0.18a$, where a is the lattice constant. The band structures are solved by means of a transfer-matrix method.

VI. WAVE TRANSMISSION AND REFLECTION IN SEMI-INFINITE 2D PHOTONIC CRYSTALS

To demonstrate the power of the developed TMM in application to semi-infinite photonic crystal structures, we will take some examples. For simplicity and brevity, we only consider 2D photonic crystal and related waveguide structures. The extension to 3D photonic crystal structures is straightforward, but needs much more time-consuming numerical efforts. The photonic crystal we study here is composed of a square lattice of dielectric cylinders embedded in an air background. The cylinder has a dielectric constant of $\epsilon = 11.56$ and a radius of $r = 0.18a$, where a is the lattice constant. The corresponding filling fraction of the cylinder is $f = 10.3\%$. For a semi-infinite photonic crystal, we assume that the surface is normal to the (10) crystallographic direction. In addition, we assume that the incident wave is at the *E*-polarization mode (with the electric field parallel to the cylinder axis), and propagates parallel to this direction. Obviously, we have considered a normal incidence situation. The incident wave will then witness the photonic band structures and band gaps along the (10) direction. We have used the TMM described in Sec. II to calculate the band structure, and the result is plotted in Fig. 6. Here 15 plane waves have been used in the calculation, and good convergence has been achieved, consistent with the fact that the *E*-polarization mode allows for fast convergency. Only eigenmodes with ω below $0.7(2\pi c/a)$ are shown, where c is the light speed in free space. There is a wide fundamental (10) directional band gap between $0.261(2\pi c/a)$ and $0.443(2\pi c/a)$. Another much narrower band gap opens between the second and third photonic bands. We have also applied the conventional plane-wave expansion method[27–29] to solve the photonic band structure, and found the same results.

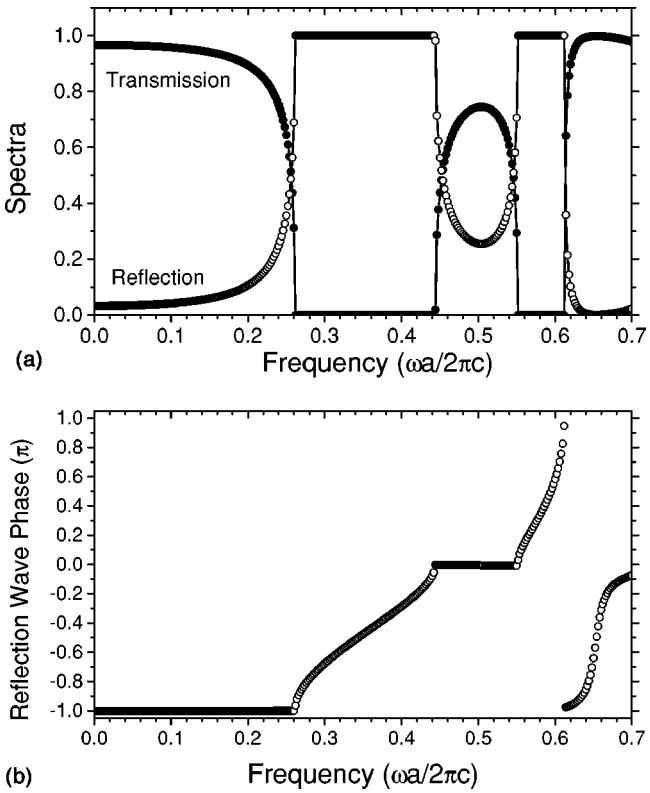

FIG. 7. (a) Calculated transmission and reflection spectra for a plane EM wave scattering by the semi-infinite 2D photonic crystal investigated in Fig. 6. The plane wave is normally incident on the surface of the crystal along the (10) direction. (b) The phase shift of the reflection wave relative to the incident wave.

Now we send a plane wave normally incident on the semi-infinite photonic crystal, in a way very closely represented by the schematic configuration shown in Fig. 1(a). We scan the frequency range between 0 to $0.7(2\pi c/a)$ by using a small step of $0.002(2\pi c/a)$. For each monochromatic incident wave, we can calculate the transmission wave propagating into the photonic crystal and the reflection wave bounced back from the crystal. The resulting spectra of the transmission and reflection coefficients are displayed in Fig. 7(a). At the frequency range of the two band gaps, the transmission coefficient is exactly zero, and the reflection coefficient is precisely 100%, as can be expected. More interesting features come from the frequency range corresponding to the photonic bands, and they show complex behaviors. At frequencies below the fundamental band gap, which ranges from 0 to $0.261(2\pi c/a)$, the transmission (reflection) coefficient shows a very simple monotonous decaying (growing) behavior. At very long wavelengths, a saturation occurs in the transmission and reflection spectra, leaving a 96.74% (3.26%) transmission (reflection) coefficient. It has been well established that a photonic crystal behaves similar to a homogeneous medium with an effective refractive index of n in the long-wavelength limit. According to the well-known Fresnel's formula $r = (1-n)/(1+n)$ and $R = r^2$. For the current photonic crystal, $R = 3.26\%$, then $r = -18.06\%$, which yields an effective refractive index of $n = 1.441$. This value is very close to that calculated by a scalar effective medium

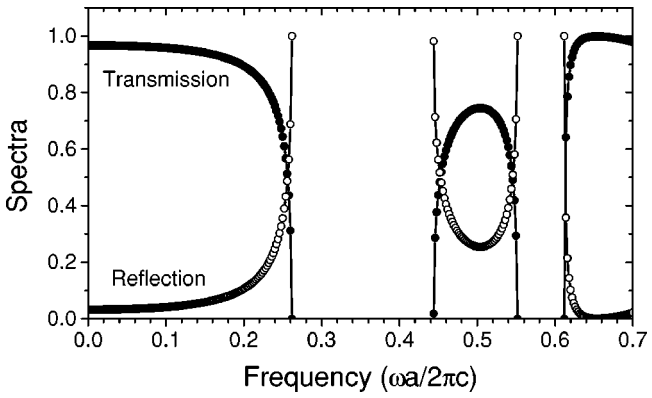

FIG. 8. Calculated transmission and reflection spectra for the inverse problem of Fig. 7, where a Bloch wave is scattered by the semi-infinite 2D photonic crystal investigated in Fig. 6. The Bloch wave is normally incident on the surface of the crystal along the (10) direction. Data in the band gaps are absent because there is no Bloch mode in these frequency ranges.

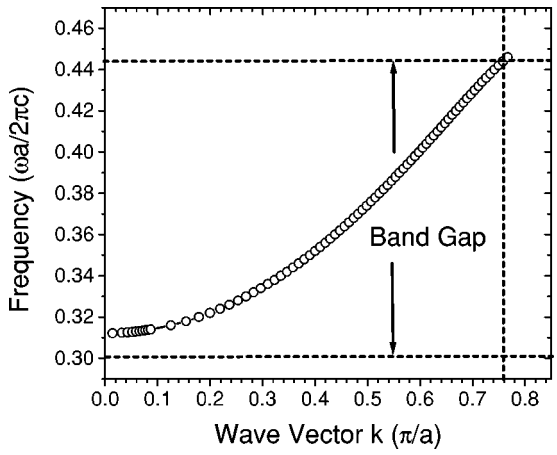

FIG. 9. Plot of the band diagram of guided modes in a waveguide created in the 2D photonic crystal investigated in Fig. 6 by removing a single row of cylinders along the (10) direction. The results are solved by means of a transfer-matrix method.

theory $n=\sqrt{f\epsilon+(1-f)}=1.445$. If we can regard the photonic crystal as an effective homogeneous medium in the whole frequency range below the fundamental band gap, then the monotonous growing behavior of R implies that the effective refractive index n increases monotonously to an infinite value at the band edge. Of course, the effective medium theory only holds in the long-wavelength limit and fails at those modest frequencies close to the band gap. At higher photonic bands the spectra show more complicated behaviors, where no monotonous variation behavior is found.

It is interesting to look at the phase of the reflection wave. In the whole frequency range considered here, the reflection wave in the far-field region only contains zero-order Bragg wave (plane wave), so it is possible to define the phase of this plane wave in reference to that of the incident plane wave. The calculated result is displayed in Fig. 7(b). In the whole frequency range below the fundamental band gap, the phase shift of the reflection wave compared to the incident wave remains at $-\pi$ (same to π). If we use the formula $r(\omega)=[1-n(\omega)]/[1+n(\omega)]$, then we find that $n(\omega)$ is always a real number larger than 1. In the fundamental band gap, the phase shift increases from $-\pi$ to 0, indicating that $n(\omega)$ is now a complex number, $n(\omega)=n_r(\omega)+in_i(\omega)$, and $r(\omega)=[1-n_r(\omega)-in_i(\omega)]/[1+n_r(\omega)+in_i(\omega)]$. This is consistent with the fact that in the band gap, the photonic crystal behaves similar to a metallic material with a complex refractive index, and the only mode that can exist is the surface evanescent mode. A similar metallic behavior can also be found in the phase-shift pattern at the second band gap. Similar to the transmission (reflection) spectra, the phase shift for higher photonic bands shows a complicated behavior, and cannot be explained by a simple parameter of $n(\omega)$. This is not hard to understand because the effective refractive index has no physical significance at short wavelengths comparable to the lattice constant of the photonic crystal.

Now let us look at the inverse problem of a Bloch wave propagating from deep inside the photonic crystal along the (10) direction scattered by the air-crystal interface, as shown in Fig. 1(b). The calculated transmission and reflection coefficients are plotted in Fig. 8 as a function of the frequency of the incident Bloch wave. Note that the data in the band gap is absent. The reason is that no Bloch modes exist in these frequency ranges, which renders the wave propagation problem meaningless. An interesting phenomenon can be found in the spectra when we compare Fig. 8 to Fig. 7(a): The spectrum curves are identical to each other. This identity of the transmission and reflection coefficients in the two inverse wave propagation problems can be understood from the time-reversal symmetry in this system. In other words, it is a natural result from the application of reciprocal theorem of light to the current purely dielectric structure. This also recalls the situation of a homogeneous glass plate with a refractive index n. The reflection coefficient for a plane wave normally incident from air onto the glass is identical to that for a plane wave normally incident from glass onto air, both are $R=r^2=(1-n)^2/(1+n)^2$. The other reason for this identity is that there is only zero-order Bragg wave existing in the air region, and only one Bloch mode can be excited in the photonic crystal, so that these two inverse problems are symmetrical when time is reversed. In more complicated situations, this identity might be broken.

VII. COUPLING OF EM WAVES INTO AND OUT OF PHOTONIC CRYSTAL WAVEGUIDES

After having gained some experience on how the TMM is applied to simple semi-infinite photonic crystal structures, we proceed to considering wave propagation in a photonic crystal waveguide structure, which is an important functional element in a photonic crystal based optical IC. The waveguide is created in the above semi-infinite 2D photonic crystal by removing a single row of cylinders along the (10) direction. One important subject about such an optical element is the coupling of EM waves into and out of the waveguide. As we discussed in the Introduction, it is of great benefit both physically and numerically to completely re-

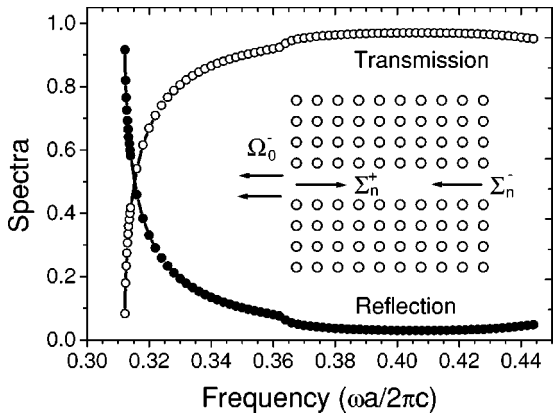

FIG. 10. Calculated transmission and reflection spectra for a guided wave coupling out of a semi-infinite 2D photonic crystal waveguide investigated in Fig. 9. The configuration of the scattering problem is depicted in the inset.

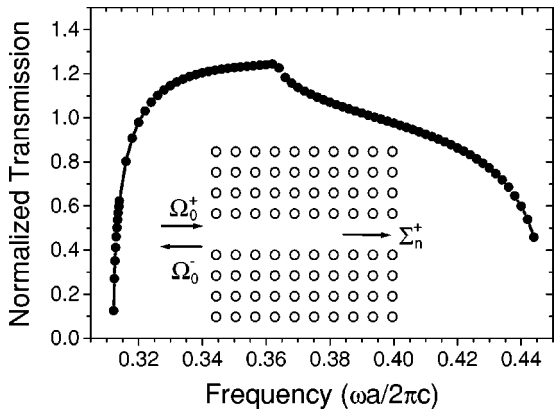

FIG. 11. Calculated normalized transmission spectrum for a plane wave coupling into the same photonic crystal waveguide as in Fig. 10. The transmission coefficient is normalized with respect to an incident total energy flux in a size of one lattice constant. Inset shows the configuration of the wave scattering problem.

move the multiple-reflection contamination to the useful information induced by the second exit in a finite-length waveguide. To achieve this, a semi-infinite waveguide is necessary and our developed TMM is perfectly suitable for this task. Unlike the above photonic crystal, we need to adopt a supercell technique in order to appreciate the transfer-matrix formalism.

In order to have a clear understanding of this problem, we first investigate the behavior of guided modes existing in such a waveguide. The band diagram of guided mode has been calculated by means of the TMM. A supercell consisting of up to 11 unit cells centered at the axis of the waveguide has been adopted, and up to 129 plane waves have been used to calculate the dispersion of the Bloch mode (guided mode) in this structure. The result is displayed in Fig. 9, where the two horizontal dashed lines denotes the edge of the complete *E*-polarization band gap of the bulk 2D photonic crystal, which lie at 0.302 and $0.443(2\pi c/a)$, respectively. A single wide guided-mode band spans monotonously from $0.312(2\pi c/a)$ at $k=0$ to the upper band edge at about $k=0.76(\pi/a)$.

The schematic configuration of guided wave coupling out of the waveguide is shown in the inset of Fig. 10. $\Sigma_n^-=(0,\ldots,0,\sigma_j^-,0,\ldots,0)^T$ is the column vector in the eigenstate space, where $\sigma_j^-=1$ is the amplitude for the negative propagating (from right to left) guided mode. When this guided mode impinges on the waveguide exit, some part is reflected back into the waveguide and finally evolves into a positive propagating (from left to right) guided mode described by $\Sigma_n^+=(0,\ldots,0,\sigma_m^+,0,\ldots,0)^T$, with σ_m^+ being the amplitude of this positive guided mode. The other part of wave transmits through the waveguide exit and dissipates into the free space in the form of Ω_0^-. Although we only consider the simple case of a waveguide connected with an air background, a more complex problem such as coupling of wave out of photonic crystal waveguides into conventional planar or slab waveguides can also be solved in the same framework. To calculate the reflection and transmission coefficients, we work in the real space instead of the *k* space. We first calculate the distribution of the electric and magnetic fields in a plane (with a size equal to the supercell) perpendicular to the waveguide axis from the knowledge of Σ_n^-, Σ_n^+, and Ω_0^-, from which the Poynting vector is calculated at each sampling point in this plane. Then the total energy flux in this plane is summed up to I_0, I_r, and I_t corresponding to the incident, reflection, and transmission energy fluxes, from which we find $R=I_r/I_0$ and $T=I_t/I_0$. The calculated reflection and transmission spectra for this waveguide are displayed in Fig. 10 by the solid and open dot curves, respectively. It can be seen that the reflection (transmission) coefficient almost monotonously decays when the frequency of the guided mode is increased. Near the waveguide cutoff frequency $[0.312(2\pi c/a)]$, the reflection (transmission) coefficient can be over 90% (below 10%), indicating very poor coupling-out efficiency. The contrary behavior is found at frequencies near the upper band edge. Here the transmission (reflection) coefficient can be as high as 97% (as low as 3%), and therefore the coupling efficiency out of the waveguide is very high.

The inverse problem of coupling an external incident wave into the waveguide (the corresponding schematic configuration is shown in the inset of Fig. 11) has also been investigated in the same theoretical framework. For simplicity, we also consider a plane wave normally incident on the waveguide. Since the incident field (Ω_0^+) is extended in space (and thus infinite in the energy flux), while the transmission field (Σ_n^+) is a localized guided wave (and thus finite in the energy flux), the transmission and reflection coefficients are ill defined. Physically it is easy to understand that most part of the incident wave is reflected back by the bulk photonic crystal, and only those waves close to the waveguide exit can go into the waveguide and evolves into a guided wave. Therefore, one more reasonable measure to monitor the coupling efficiency is to look at a normalized transmission coefficient, which is defined to be the ratio of the total transmission energy flux to the total incident energy flux in a sampling region whose width is equal to the apparent width of the waveguide (*a* for the current structure). The normalized transmission coefficient as a function of the inci-

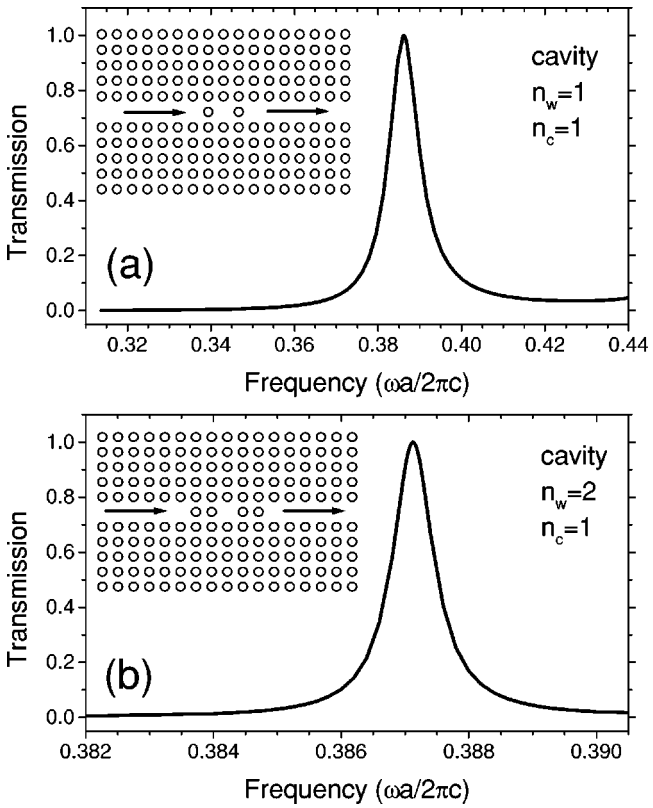

FIG. 12. Transmission spectra for a guided wave scattered by a cavity (with a size of one unit cell) introduced into a 2D photonic crystal waveguide. The schematic configurations of the waveguide and the cavity are depicted in the insets.

dent wave frequency has been calculated and the result is plotted in Fig. 11. In contrast to the monotonous variation in Fig. 10, the transmission spectrum shows a more complex feature. A peak stands around frequency $0.36(2\pi c/a)$, where the efficiency can reach 120%, indicating a slight focusing effect. The coupling-in efficiency is very bad near the waveguide cutoff frequency, similar to the behavior of the coupling-out efficiency. Another significant difference between the two processes lies at frequencies near the upper band edge. While the coupling-out efficiency is close to 100%, the coupling-in efficiency is below 80%. This might be attributed to the mismatch of a uniform field profile of the incident plane wave with that of a localized guided wave in this frequency range. We have found that much better coupling-in efficiency can be achieved by careful design of the incident wave profile. For example, a Gaussian beam can improve the coupling-in efficiency remarkably.

VIII. WAVE PROPAGATION IN SANDWICHED PHOTONIC CRYSTAL WAVEGUIDE STRUCTURES

In the above two sections we have discussed the solution of wave propagation in semi-infinite 2D photonic crystal and related waveguide structures. Now we go one step further to look at more complicated sandwiched photonic crystal and related waveguide structures. We will take a functional element in an optical IC, cavities created in a straight photonic crystal waveguide,[30,31] as an example to demonstrate the principle and power of the developed TMM

The first structure we study is schematically shown in the inset of Fig. 12(a). The basic structure is a straight photonic crystal waveguide that has been discussed in Sec. VII with parameters of $\epsilon=11.56$ and $r=0.18a$. Excitation of an *E*-polarization mode is also assumed. A cavity can be introduced into this background waveguide by placing two symmetric walls made up of dielectric cylinders. These cylinders have the same geometrical and physical parameters as the other cylinders building the background photonic crystal, and are located in the lattice sites of the background crystal. The cavity is characterized by two geometric parameters n_w and n_c, which denotes the layer number of each wall and the layer number occupied by the central vacant region between the two walls. Therefore, n_w and n_c are parameters determining the wall thickness and size of the cavity. In the current structure, $n_w=1$ and $n_c=1$, namely, the cavity is one unit-cell wide, and the wall is one unit-cell thick. Suppose a guided wave is sent propagating from left to right and impinges on the cavity, the question is to find out the transmission and reflection coefficients.

To find the answer to this question, we first adopt a supercell to place the wave propagation problem into the TMM framework. Next we look upon the central cavity as a grating slab three unit cells thick sandwiched between two semi-infinite photonic crystal waveguides. After this, we can directly utilize the formalisms described in Sec. V to calculate the transmission and reflection coefficients. The key is to solve the eigenmodes of the two identical semi-infinite waveguides (including two guided modes and many evanescent modes) as well as the *S* matrix for the grating slab. The result of the transmission spectra is plotted in Fig. 12(a) for a wide frequency range almost covering the whole guided-mode band. A single peak is found with the resonance occurring at frequency $\omega_0=0.3862(2\pi c/a)$. The full width at half maximum (FWHM) of the peak is about $\Delta\omega=0.009(2\pi c/a)$. From these two physical parameters we can calculate the quality factor (Q factor) of this cavity, which is $Q=\omega_0/\Delta\omega\approx 43$. Naively one can imagine that this transmission peak is induced by the cavity mode coupling with the incident guided wave. In fact, we have calculated the localization mode involved in this cavity (with infinitely thick walls) by means of the conventional plane-wave expansion method.[27–29] Using a supercell composed of 7×7 square unit cells and up to 3000 plane waves, we find a single cavity mode located at an eigenfrequency of $\omega=0.3870(2\pi c/a)$, very close to the transmission spectrum calculation. One important point about the spectrum is that the signal is very clean, completely free from usual dense interference pattern (induced by multiple reflection from the two waveguide exits in a usual waveguide of finite length) superimposed onto the envelope of the useful signal. The mere reason is that two semi-infinite waveguides are adopted, and there is no structural boundaries (the waveguide exits) present.

We can change the geometrical parameters of the sandwiched cavity structure to modify its optical properties. Figure 12(b) shows the transmission spectrum for a cavity with

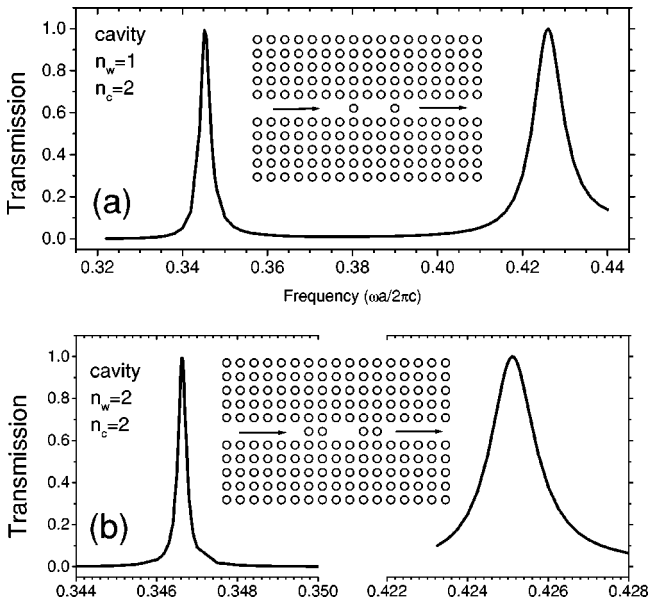

FIG. 13. Same as in Fig. 12, except the cavity is now of a size of two unit cells.

$n_w=2$ and $n_c=1$. Since the thickness of the wall of the cavity is doubled, we expect that the Q factor of the cavity will be significantly enhanced. Indeed Fig. 12(b) has fully validated this assumption. Now the resonance peak is located at $\omega=0.3871(2\pi c/a)$, a slight blueshift compared to the resonance peak in Fig. 12(a) for $n_w=1$. The FWHM of this new peak is found to be about $0.0008(2\pi c/a)$, leading to a Q factor of about 484, over 10 times larger than the Q factor of the cavity with $n_w=1$. It is expected that when the wall of the cavity is further increased, its Q factor will continue to grow, basically following an exponential law. In these structures the introduction of a cavity can serve as an efficient filter to the wide-band guided wave.

In addition to changing the thickness of the wall of the cavity, we can also adjust the size of the vacant space of the cavity. It is expected that fine tuning of the resonance frequency can be easily achieved. Figures 13(a) shows the transmission spectrum for a cavity with $n_w=1$ and $n_c=2$ (as schematically depicted in the inset) in a wide frequency range. The space of the cavity has been increased to occupy two unit cells. Consequently two resonance peaks appear, with the lower one centered at $\omega_1=0.3452(2\pi c/a)$, while the higher one centered at $\omega_2=0.4260(2\pi c/a)$. We also carry out solution of the localization modes involved in this cavity (also with infinitely thick walls), and find two cavity mode located at frequency $0.3451(2\pi c/a)$ and $0.4258(2\pi c/a)$, respectively, also very close to the transmission spectrum calculation. This means that the two transmission peaks definitely come from the resonance coupling with the cavity modes.

The two transmission peaks almost has an equal distance to the peak [centered at $\omega_0=0.3862(2\pi c/a)$] for the smaller cavity with $n_c=1$ in Fig. 12, indicating that the two new resonance peaks might origin from symmetric splitting of the old single peak due to a size effect. The FWHM for these two resonance peaks are $0.0028(2\pi c/a)$ and $0.009(2\pi c/a)$, corresponding to a Q factor of 123 and 47, respectively. Clearly the two peaks are quite asymmetric in their optical properties. We also increase the thickness of the wall of this cavity, and the calculated transmission spectrum is displayed in Fig. 13(b) for $n_w=2$ and $n_c=2$ (whose geometry is shown in the inset). For clarity of eyeview, only spectra around the resonance peaks are shown here. Similar to the smaller cavity in Fig. 12, the resonance peaks in the current cavity become much narrower. The peaks are now centered at $\omega_1=0.3466(2\pi c/a)$ and $\omega_2=0.4251(2\pi c/a)$, slightly blueshift and redshift, respectively, from the two peaks for the cavity with thinner wall of $n_w=1$. The FWHM for the two peaks are reduced to values of $0.00024(2\pi c/a)$ and $0.0014(2\pi c/a)$, and the corresponding Q factors are about 1444 and 304, respectively. Obviously the lower resonance peak is much finer than the higher peak. This phenomenon might be related to the fact that the distance of the lower peak away from the lower PBG edge $[0.302(2\pi c/a)]$ is much larger than the distance of the higher peak away from the higher PBG edge $[0.443(2\pi c/a)]$, and therefore is more localized around the waveguide.

IX. FURTHER DISCUSSIONS ON TMM IN APPLICATION TO PHOTONIC CRYSTAL FUNCTIONAL ELEMENTS

It is interesting to make some comparisons between the developed TMM and the more popular FDTD approach. The FDTD approach can efficiently govern the dynamics (time evolution) of EM wave propagation in complex structures, and has been dominantly utilized in theoretical understanding of the optical properties of many important functional elements built in a photonic crystal platform, such as waveguide, waveguide bends and branches, and cavities. Other reasons that greatly contribute to the popularity of the FDTD approach are its simplicity in essence, ease of computational memory-space requirement, and ability to handle any complex structure, either periodic or aperiodic.

However, the FDTD approach also exhibits some intrinsic weaknesses when applied to treat the spectrum of scattering problems in a closed system (where the background is not free space but rather an extended inhomogeneous medium such as a photonic crystal). In the scheme of pulse excitation, in order to have a very fine frequency resolution, as is required for the current resonance scattering problems, the input pulse needs to be very long. However, this is in contrast to the adoption of a finite simulation domain and consequent multiple reflection from the structural boundaries. To obtain a reasonable result for the spectrum, the parasite reflection pulses from the boundary must be in sufficient separation from other useful pulses. This in turn requires a sufficiently large simulation domain size. The contrast can only be efficiently solved by increasing the structure size. An infinite structure (such as the semi-infinite photonic crystal waveguides studied in the above sections) should be most welcomed, but unfortunately it has not been seriously considered (or perhaps hard to be implemented) in the FDTD technique. These practical weaknesses suggest that people be more careful in extracting very quantitative information about the spectrum for a closed system such as the above

waveguide-cavity sandwiched structures. In contrast, open-system related problems such as wave scattering by a space-limited object placed in free space are not subject to these weaknesses.

The developed TMM can overcome the shortcomings of the FDTD scheme in application to those closed systems. First, since it is working in the frequency domain, there is no difficulty of frequency resolution. Therefore, it is the best candidate for the purpose of spectrum calculation in a wave scattering problem. Second, since we have developed models to match the semi-infinite photonic crystal structures, the difficulty of multiple-reflection induced contamination to the useful spectrum no longer exists. This makes it more competitive to handle the spectrum for wave scattering in a closed system than the FDTD techniques. Yet, one disadvantage of the TMM is that the computational memory-space requirement (which is proportional to the square of the plane wave number) is far larger than in the FDTD approach (which is linearly proportional to the pixel number in real space and the time step used). Another more serious disadvantage is that the current formulation of the TMM is limited to periodic structures, or structures that can be approximated by an artificial periodic system (where a supercell technique can be utilized). Extension of the formulation to aperiodic functional elements in an optical IC should be invaluable.

Finally we would like to point out that the TMM can provide a better environment for designing new optical functional elements than the FDTD technique can. Take the cavity problem discussed in Sec. VIII as an example. Suppose we wish to design an efficient element only through adjustment of the geometrical and physical parameters of the small cavity region. Then in the framework of the TMM, each time we only need to change the S matrix for the sandwiched slab occupied by the cavities, other physical quantities such as the eigenmodes in the background two semi-infinite waveguide structures can be stored and used as many times as one would like once they have been calculated. Obviously, the numerical burden is limited to the small sandwiched region. The situation is completely different in the FDTD scheme. Every time one changes the parameters (no matter how little), one needs to run the numerical calculation once again in the whole simulation domain, which in most cases is far larger than the sandwiched slab. This limitation surely will bring great inconvenience to active design of functional elements in a photonic crystal background. The same situation also exists in the waveguide coupling problem discussed in Sec. VII.

X. SUMMARY

In summary, we have developed a TMM that is based on the plane-wave expansion of EM fields to handle EM wave propagation in semi-infinite photonic crystal and related waveguide structures. One great advantage for this TMM is that it enables one to focus only on wave scattering at the concerned structural boundary and to completely remove the contamination due to multiple reflections in the presence of other structural boundaries. We have found that the wave scattering problem is closely connected to the eigenmodes of the transfer matrix for the unit cell of the photonic crystal. We have imposed a natural boundary condition to describe the asymptotic propagation behavior of scattered EM waves in a region far away from the scattering region. This has efficiently accounted for the physical information of EM wave propagation in the inhomogeneous background materials, periodic photonic crystals, and related waveguide structures here. Several numerical schemes have been implemented to efficiently and accurately solve the eigenmodes for the transfer matrix. In this eigenstate space, EM wave will not encounter any scattering when propagating through the photonic crystal. This basis brings significant simplification to the solution of the wave propagation problem.

We have considered several general structures in conjunction with a semi-infinite photonic crystal, and evaluated the corresponding theoretical tools. These include wave propagation in a semi-infinite photonic crystal, a coated semi-infinite photonic crystal, a heterostructure formed by two different semi-infinite photonic crystals face to face, and a more complex sandwiched structure formed by two semi-infinite photonic crystals separated by a general grating slab. In combination with a supercell technique, the developed formalisms can also be used to handle photonic crystal waveguide structures. We have applied the developed theoretical tools to investigate 2D photonic crystal and related waveguide structures under the excitation of the E-polarization mode. We first consider the simplest situation of a plane wave propagation into a 2D photonic crystal and the corresponding inverse problem of a Bloch's wave propagation out of the photonic crystal. Then we turn to the problem of EM wave coupling into and out of a photonic crystal waveguide. Both the coupling-in and coupling-out efficiencies have been addressed. We then look at wave propagation in more complicated sandwiched photonic crystal waveguide structures. The structure we study is a cavity introduced into a photonic crystal waveguide. This cavity can act as a frequency filter to a continuous spectrum of guided wave. We have changed the geometrical configurations of the cavity and examined its optical properties in the environment of the photonic crystal waveguide.

The developed TMM can have advantage over the popular FDTD approach in extracting accurate spectrum information of wave scattering in closed systems of functional elements embedded in an extended inhomogeneous medium background such as a photonic crystal. In addition, the TMM is more competent and convenient to actively design new optical functional elements created in a photonic crystal background than the FDTD approach does. It is expected the developed TMM can help people to understand complicated wave propagation behavior in individual functional elements comprising an optical IC built in a photonic crystal platform, and then design optimal optical elements to realize applications in a wide range. It is also expected that the power of this efficient theoretical tool and its advantage over other numerical tools will be witnessed more fully in handling complex 3D photonic crystal functional elements.

ACKNOWLEDGMENTS

Ames Laboratory is operated for the U.S. Department of Energy (DOE) by Iowa State University under Contract No. W-7405-Eng-82.

*Electronic address: lizy@axel.ameslab.gov

[1] E. Yablonovitch, Phys. Rev. Lett. **58**, 2059 (1987).
[2] J.D. Joannopoulos, P.R. Villeneuve, and S. Fan, Nature (London) **386**, 143 (1997).
[3] A. Mekis, J.C. Chen, I. Kurland, S. Fan, P.R. Villeneuve, and J.D. Joannopoulos, Phys. Rev. Lett. **77**, 3787 (1996).
[4] S.Y. Lin, E. Chow, V. Hietala, P.R. Villeneuve, and J.D. Joannopoulos, Science **282**, 274 (1998).
[5] S.G. Johnson, P.R. Villeneuve, S. Fan, and J.D. Joannopoulos, Phys. Rev. B **62**, 8212 (2000).
[6] A. Chutina and S. Noda, Phys. Rev. B **62**, 4488 (2000).
[7] M. Tokushima, H. Kosaka, A. Tomita, and H. Yamada, Appl. Phys. Lett. **76**, 952 (2000).
[8] E. Chow, S.Y. Lin, S.G. Johnson, P.R. Villineneve, J.D. Joannopoulos, J.R. Wendt, G.A. Vawter, W. Zubrzycki, H. Haus, and A. Allenman, Nature (London) **407**, 983 (2000).
[9] A. Chutina and S. Noda, Appl. Phys. Lett. **75**, 3739 (1999).
[10] D. Nedeljkovi, T.P. Pearsall, S.A. Kuchinsky, M.D. Mikhailov, M. Lonar, and A. Scherer, in *Nanoscale Linear and Nonlinear Optics: International School on Quantum Electronics*, edited by M. Bertolotti, C.M. Bowden, and C. Sibilia, AIP Conf. Proc. No. 560 (AIP, Woodbury, 2001), p. 107.
[11] T.F. Krauss, in *Nanoscale Linear and Nonlinear Optics*: *International School on Quantum Electronics*, edited by M. Bertolotti, C. M. Bowden, and C. Sibilia, AIP Conf. Proc. No. 560 (AIP, Woodbury, 2001), p. 89.
[12] Y. Sugimoto, N. Ikeda, N. Carlsson, K. Asakawa, N. Kawai, and K. Inoue, J. Appl. Phys. **91**, 922 (2002).
[13] M. Bayindir, E. Ozbay, B. Temelkuran, M.M. Sigalas, C.M. Soukoulis, R. Biswas, and K.M. Ho, Phys. Rev. B **63**, 081107 (2001).
[14] Z.Y. Li and K.M. Ho, J. Opt. Soc. Am. B **20**, 801 (2003).
[15] A. Taflove and S.C. Hagness, *Computational Electrodynamics: The Finite-Difference Time-Domain Method* (Artech House, Boston, 2000).
[16] A. Mekis, S. Fan, and J.D. Joannopoulos, IEEE Microw. Guid. Wave Lett. **9**, 502 (1999).
[17] J.B. Pendry, J. Mod. Opt. **41**, 209 (1994).
[18] P.M. Bell, J.B. Pendry, L. Marin Moreno, and A.J. Ward, Comput. Phys. Commun. **85**, 306 (1995).
[19] L.C. Botten, N.A. Nicorovici, R.C. McPhedran, C. Martijn de Sterke, and A.A. Asatryan, Phys. Rev. E **64**, 046603 (2001).
[20] Z.Y. Li and K.M. Ho, Phys. Rev. B **67**, 165104 (2003).
[21] M.G. Moharam, E.B. Grann, D.A. Pommet, and T.K. Gaylord, J. Opt. Soc. Am. A **12**, 1068 (1995).
[22] L. Li, J. Opt. Soc. Am. A **13**, 1870 (1996).
[23] L. Li, J. Opt. Soc. Am. A **13**, 1024 (1996).
[24] E. Silberstein, P. Lalanne, J.P. Hugonin, and Q. Cao, J. Opt. Soc. Am. A **18**, 2865 (2001).
[25] B. Gralak, S. Enoch, and G. Tayeb, J. Opt. Soc. Am. A **19**, 1547 (2002).
[26] Z.Y. Li and L.L. Lin, Phys. Rev. E **67**, 046607 (2003); L.L. Lin, Z.Y. Li, and K.M. Ho, J. Appl. Phys. **94**, 811 (2003).
[27] K.M. Ho, C.T. Chan, and C.M. Soukoulis, Phys. Rev. Lett. **65**, 3152 (1990).
[28] D. Cassagne, C. Jouanin, and D. Bertho, Phys. Rev. B **53**, 7134 (1996).
[29] Z.Y. Li, J. Wang, and B.Y. Gu, Phys. Rev. B **58**, 3721 (1998); Z.Y. Li, B.Y. Gu, and G.Z. Yang, Phys. Rev. Lett. **81**, 2574 (1998).
[30] C.J.M. Smith, R.M. De La Rue, M. Rattier, S. Olivier, H. Benisty, C. Weisbuch, T.F. Krauss, R. Houdre, and U. Oesterle, Appl. Phys. Lett. **78**, 1487 (2001).
[31] J. Moosburger, M. Kamp, A. Forchel, U. Oesterle, and R. Houdre, J. Appl. Phys. **91**, 4791 (2002).